

Performance of microdosimetric detectors using Monte-Carlo

Filipe Ficalho^{1,a}

¹Instituto Superior Técnico, Lisboa, Portugal

Project supervisor: J.G. Saraiva and Cristiana Rodrigues

November 13, 2022

Abstract. The paper describes a study aiming at the development of microdosimeters using electrospun micrometric scintillating plastic optical fibres (SPOF) ($<25\mu\text{m}$). Using TOPAS-MC Monte Carlo simulations, including the simulation of the scintillation process, and using different fibre dispositions layouts are made. The SPOFs are placed in hexagonal arrangements, close-packed (7 and 91 fibres) and separated by $25\mu\text{m}$ air gaps (only for 7 fibres).

KEYWORDS: microdosimetry, TOPAS, Monte-Carlo, scintillating fibers

1 Introduction

1.1 Proton Therapy

Proton therapy is an alternative treatment to conventional radiation therapy, used to treat many kinds of tumors and cancers. What makes this treatment interesting is the appearance of an energy density (dE/dx) spike at a well-defined depth (Bragg's peak) related to the protons' kinetic energy. Conventional radiation therapy is done using a photon beam to apply radiation to the tumor. Unfortunately, the beam needs to reach a considerably larger absorbed dose on the surrounding healthy tissue to hit the tumor with the prescribed dose. The different responses from these two types of beams are shown in figure 1, showing how much radiation dose ($\propto dE/dx$) is deposited in the tumor and the surrounding regions. [1]. Photons can only be completely absorbed, or not deposit any energy at all. On the other hand, protons deposit part of their energy as they penetrate materials. The proton-deposited energy is related to the crossed path traveled within a certain medium. The lower energy a proton has, the more energy it deposits in the material per unit of crossed path. This ultimately results in the Bragg peak for the energy density when protons reach the penetration range in a medium. Tuning the beam energy, i.e. protons' kinetic energy, one can change the location of the Bragg peak e.g. to irradiate a specific organ in the human body. To monitor the radiation dose delivered to a patient are necessary detectors (either actively with e.g. scintillating fibers or passively with e.g. doped sapphire detectors) able to describe how much energy is deposited by the protons. For the microdosimetric scale, these measurements should be achieved with high precision and resolution ideally reaching tenths of μm . A possible solution to measure in real-time the deposited dose is using scintillating optical fibers. Using electrospin technology is possible to produce fibers with cross-sections of the order of tenths of μm , way smaller than the $200\mu\text{m}$ commercially available. The questions to answer in preliminary studies are: how will these fibers behave? can efficient detectors be built using these fibers? To answer these questions the simulation of the micromet-

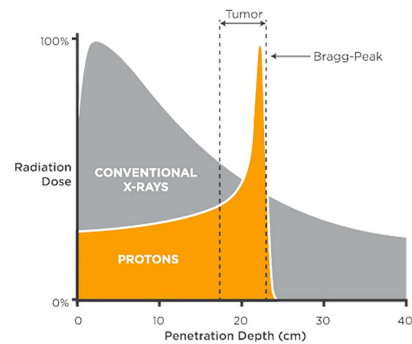


Figure 1. Radiation dose deposited in different depths for conventional radiotherapy and proton therapy. Adapted from [1]

ric fibers is developed to conclude whether they suit the role intended for them.

1.2 Scintillation

When semiconducting or insulating materials absorb energy from ionizing radiation, free electrons and holes get excited and then trapped in defects of the material or higher energy molecular orbitals. After the excitation is removed the decay into lower energy states will occur through vibrational relaxation and/or decay to lower energy orbitals. The deexcitation releases energy through the emission of photons called *scintillation photons*. Due to the loss of energy through vibrational relaxation, it is expected that the energy of the photons that are emitted is lower than the energy deposited in the material. The process of scintillation is a type of fluorescence. There is another process of scintillation called phosphorescence. In phosphorescence, an electron from a singlet state gets excited to an energetically favorable triplet-excited state, leading to an inversion of the electron's spin. This electron then decays into the singlet state, inverting its spin once again. Additionally, more energy is dissipated by non-radiative processes during phosphorescent relaxation than in fluorescence, leading to more energy being dissipated. Another important difference between these two types of scintillation is the electron's decay time. While

^ae-mail: filipe.ficalho@tecnico.ulisboa.pt

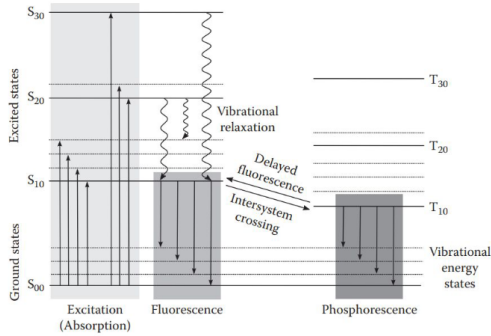


Figure 2. Schematic representation of the scintillation processes. Adapted from [3]

in fluorescence the electron decays within nanoseconds after the excitation, in phosphorescence it takes milliseconds for the decay to happen. The fluorescence signal is much faster than the one produced by phosphorescence [2] [3] and for this reason, used for radiation detection. Both of these processes are represented in figure 2.

1.3 Total Reflection

When light traveling in a medium finds a boundary that separates it from another medium three processes may occur: reflection, refraction, or absorption. Refraction is the redirection of the light as it changes its propagation medium and it is described using Snell's law (Eq. 1), which states that the ratio of the sines of the angle of incidence θ_1 and angle of refraction θ_2 is equal to the ratio of phase velocities (v_1 / v_2) for two media, or equivalently, to the refractive indices (n_2 / n_1) of the two media.

$$\frac{\sin(\theta_1)}{\sin(\theta_2)} = \frac{v_1}{v_2} = \frac{n_1}{n_2} \quad (1)$$

A particular result from this law is the total reflection occurring when the incident light meets the condition:

$$\theta_c = \arcsin(n_2/n_1) \quad (2)$$

For θ_c the incident ray is refracted with an angle of 90° , being propagated in the boundary between the materials. If the angle is further increased, the light will be refracted back into the material, being completely reflected and not being able to leave it. The different processes are illustrated in figure 3, being the total reflection the basic principle through which light is trapped within an optical fiber core volume. Throughout this text, the fibers that underwent total reflection will be referred to as "trapped".

2 Monte Carlo Simulation

Monte-Carlo simulations are used to evaluate the performance of a hypothetical microdosimeter build-up by making close-packed or air-gaped arrangements of electrospun SPOFs with diameters of the order of tenths of

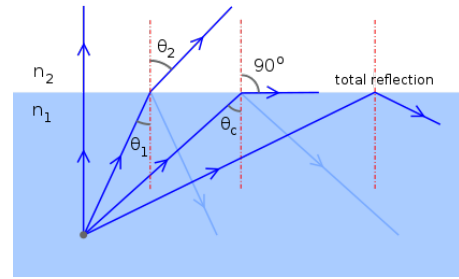


Figure 3. Schematic representation of total reflection. Adapted from [4]

micrometers while being irradiated with a proton beam. In this early study, the main goal is to determine the dimensions (length), adequate fibers layout, and efficiency of this detector. TOPAS-MC version 3.7[5, 6] (a GEANT4-based Monte Carlo tool) is used for this purpose. The simulation environment uses the following physics lists:

- g4optical
- g4em-standard_opt4
- g4h-phy_QGSP_BIC_HP
- g4decay
- g4ion-binarycascade,
- g4h-elastic_HP
- g4stopping
- g4n-trackingcut
- g4em-extra
- g4radioactivedecay
- Auger, auger cascades, fluorescence, particle induced X-ray emission are also enabled.

The *world* is a cube of air with a side of 30 cm. In the *world* are laid out the fibers made of polystyrene ($n = 1.58654$ [7]), with a cylindrical shape, a radius of 12.5 μm , and a length of 5 cm. Several of these fibers are then laid out on different arrangements to compare the geometry layout performance. Associated to the fiber material a typical scintillation spectra with a yield of 8k ph/MeV is included. The fibers are irradiated with a 150 MeV monoenergetic proton beam positioned 15 mm away from the fiber arrangement geometric center. The protons propagate along the -x direction, hitting the fibers laterally. The orientations of beam direction and fiber disposition can be depicted in figure 5). The beam shape and particle directions are described by Gaussian distributions. The proton beam field has a radius of 2.5 cm at the origin. Simulations with 1k, 5k, 10k, 50k, 100k, and 500k protons for two different setups and data analyzed with ROOT version 6.18.04[8]. These setups and the results obtained will be presented and described in sections 2.1 and 2.2. The generic simulation setup is depicted in figure 4.

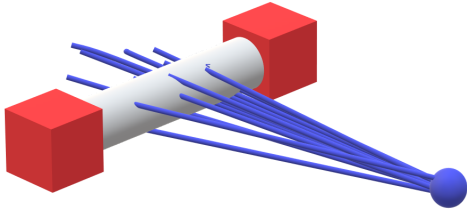


Figure 4. Rough illustration of the simulated setup. The agglomerates of scintillating fibers are represented as a gray cylinder (sensitive volume). The sensitive volume could be a set of juxtaposed fibers or spaced embedded into a tissue-equivalent phantom. Photo-detectors are represented in red. The proton beam propagates towards the sensitive volume along a direction perpendicular to its length. Image made using Paint 3D[9]

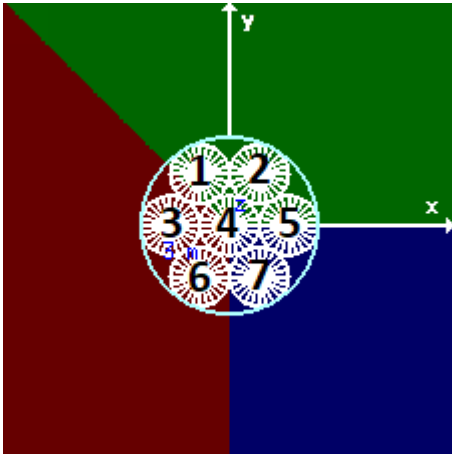


Figure 5. Layout of the fibers in their closed-packed disposition in TOPAS-MC. The Proton beam comes from the right with its center on the x-axis. The fibers are numbered to identify them and are circled by a virtual surface whose purpose is only to identify the particles that leave the agglomerate

2.1 First setup: 7 fibers in hexagonal close-packed shape

The fibers are close-packed, juxtaposed, and laid out in a hexagonal shape, as to minimize the space between the fibers, as shown in figure 5. The fibers are numbered from 1 to 7 to identify them during the data analysis. The light blue surface that envelops the fibers is not a physical surface that is being simulated but just an auxiliary surface that is used to identify which particles enter or exit the agglomerate and will be referred to as the "exit surface".

2.1.1 Deposited energy per fiber and scintillation photons created

The results for a simulation with 50k protons are shown in figures 6 and 7. Since the fibers are really small when compared with the field of the beam and due to the proton beam energy, it is expected that there should be a uniform deposition of energy in all the fibers. Figure 6, shows a non-uniformity as fibers 1 and 4 have 10% more energy

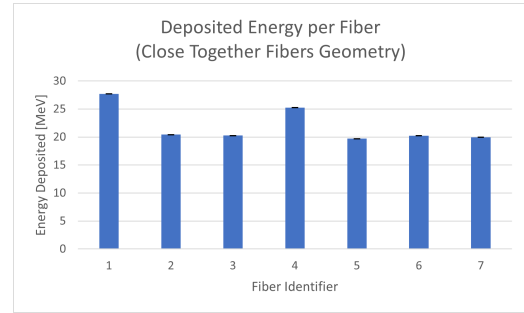


Figure 6. Deposited energy per fiber in their close-packed disposition with the respective error bar represented in black

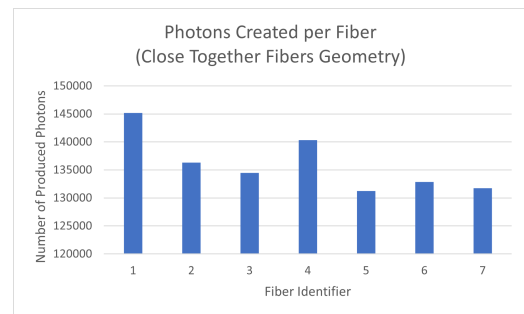


Figure 7. Scintillation photons created by each fiber in the close-packed disposition

Table 1. Fit results for the total deposited energy vs. detected photons relation in the fibers' close-packed layout

$$N = m \cdot E + b$$

m	$48893 \pm 4382.124 \text{ MeV}^{-1}$
b	42316.3 ± 24359.9
Correlation	0.999878

deposited than the other fibers. These results may be due to: (i) statistic fluctuations in the distribution of the protons due to the beam's field size (ii) the small statistics simulated (iii) any error on the simulation parameters definition. Figure 7 shows how many scintillation photons are created in each fiber. As expected, this histogram follows the same pattern as the previous histogram (in figure 6). This is in agreement with the expected performance of a scintillator with proportionality between the deposited energy and the number of scintillating photons being produced.

2.1.2 Scintillation yield and trapping efficiency

In order to make a prediction of the light collection and transport efficiency in the micrometric fibers the setup described in sections 2 and 2.1, simulation with 1k, 5k, 10k, 50k, 100k and 500k protons are produced. The results are summarized in figure 8. From a linear fit to the data the results shown in Table 1 are obtained. Where N is the number of photons that reached the photo-detector and E is the total energy deposited in the fibers. A linear relation, evidenced by the correlation ≈ 1 is observed. The

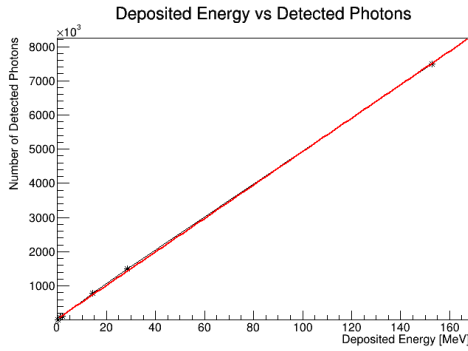


Figure 8. Total deposited energy vs. number of photons that reach the detector in the close-packed layout

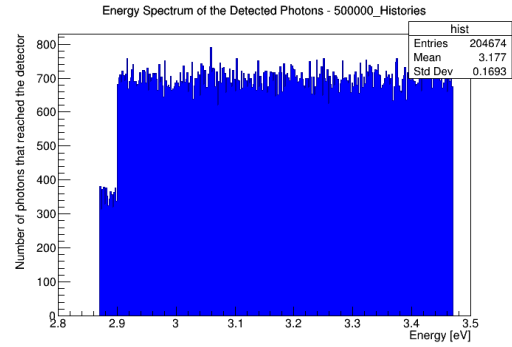


Figure 10. Energy Spectrum of the photons that were produced in the fibers and reached the photo-detector through successive total reflections

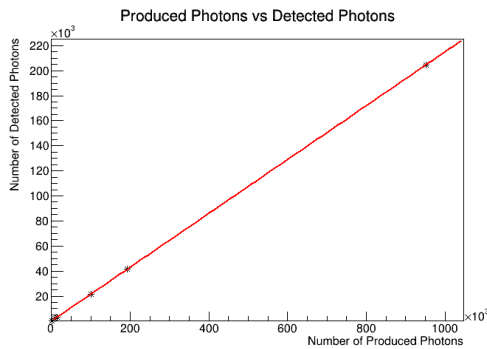


Figure 9. Total photons produced vs. number of photons that reach the detector in the close-packed layout

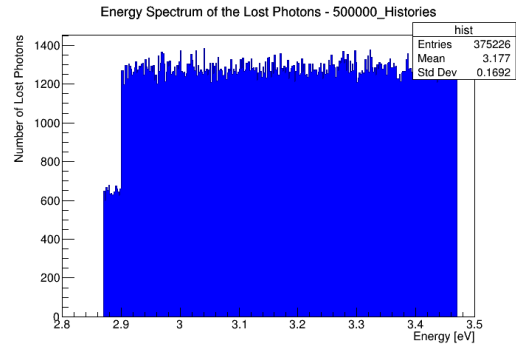


Figure 11. Energy Spectrum of the photons that fled the agglomerate of fibers through the "escape surface"

Table 2. Fit results for the total produced photons vs. detected photons relation in the fibers' close-packed layout

$$N_d = m \cdot N_p + b$$

m	$0.214877 \pm 8.69245e-05$
b	106.763 ± 34.6613
Correlation	≈ 1

fibers' trapping efficiency determines the signal collection efficiency of the fiber detector. This quantity is obtained from the relation of the number of detected photons with the number of scintillating photons produced as shown in figure 9. From a linear fit to the data are obtained the results presented in Table 2. Where N_d is the number of photons that reached the photo-detector and N_p is the number of photons produced in the fibers. The fibers' trapping efficiency is (approximately) independent of the number of photons that hit them and is given by the slope from the linear fit to the data with a value of $21.488\% \pm 0.009\%$.

2.1.3 Detected Photons' and "Lost" Photons' Spectra

One can then wonder: are there preferential photon energies to be trapped in the fibers or to escape them? To answer this question the energy spectrum of the photons that reach the ends of the fibers (shown in figure 10) is compared with the spectrum of photons that escape the agglomerate of fibers through the auxiliary surface rep-

resented in light blue on figure 5 (shown in figure 11). Observing both spectra it was concluded that there are no preferential photon energies to either leave the fibers or to get trapped in them since both show an identical interval of energies. The factors that determine the loss of photons are mainly optical and related to the diameter of the fibers and the absence of a cladding (as in commercial fibers with a cladding to improve the trapping efficiency). It should be added that for the simulations, the scintillation was set to have uniform emission spectra which is not realistic but fits the purpose of validating the scintillation process in the TOPAS-MC environment. The uniform spectrum is observed for almost all the energy ranges except for a jump in the number of photons with an energy lower than 2.9 eV. This is an issue to be investigated and understood later on and will not be covered in the following sections and is kept here for reference.

2.2 Second setup: 7 fibers in hexagonal shape with 25 μm air gaps

The fibers are laid in a hexagonal shape, separated by 25 μm (the diameter of one fiber) air gaps, as shown in figure 12. The gray lines represent the *world* made of air where the fibers are placed.

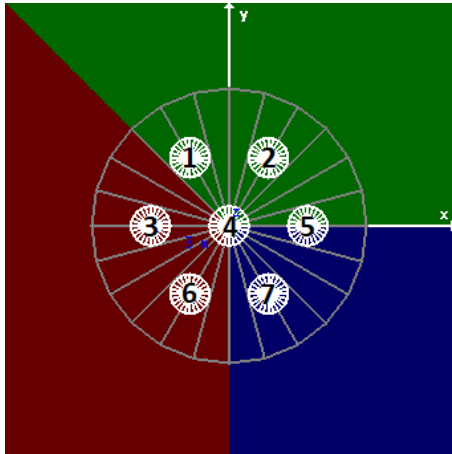


Figure 12. Layout of the fibers in their air gaps disposition in TOPAS-MC. The fibers are numbered as to identify them and are circled by a virtual surface whose purpose is only to identify the particles that leave the agglomerate

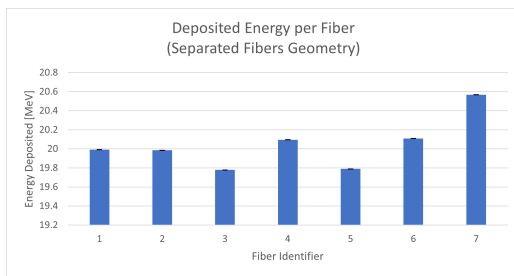


Figure 13. Deposited energy per fiber in their air gaps disposition with the respective error bar represented in black

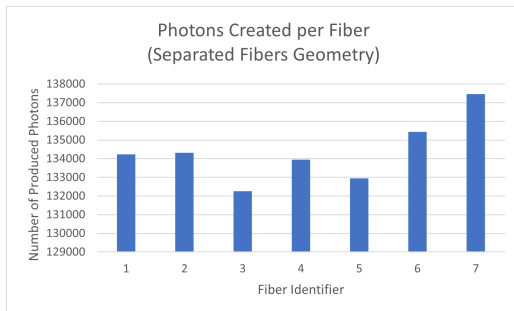


Figure 14. Scintillation photons created in each fiber for the air gaps disposition

2.2.1 Deposited Energy per fiber and Scintillation Photons

The total energy deposited in each fiber and the number of scintillation photons being produced are stored for a simulation with 50k events. In figure 13 the energy deposited for the various fibers is presented. The discrepancies observed in section 2.1.1 are now much smaller and almost negligible if attention is drawn toward the values instead of the shape of the graph.

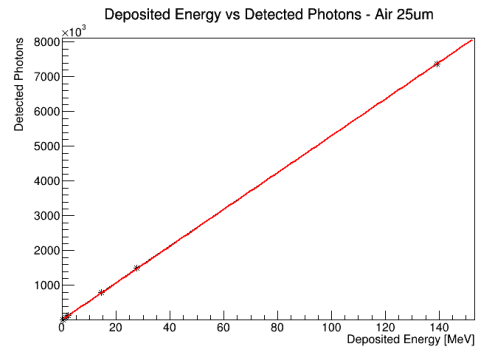


Figure 15. Total deposited energy vs. number of photons that reach the detector in the air gaps layout

Table 3. Fit results for the total deposited energy vs. detected photons relation in the fibers' air gaps layout

$$N = m \cdot E + b$$

m	$52890.8 \pm 124.024 \text{ MeV}^{-1}$
b	16264.2 ± 7223.88
Correlation	0.999989

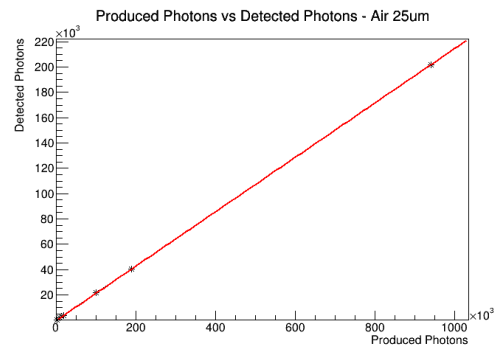


Figure 16. Total photons produced vs. number of photons that reach the detector in the air gaps layout

2.2.2 Scintillation yield and trapping efficiency

Just like in section 2.1.2, the total number of detected scintillation photons are plotted as a function of the total energy deposited in every fiber for different numbers of simulated protons (1k, 5k, 10k, 50k, 100k protons), as to look for the relation between the two variables. The results are summarized in figure 15. From a linear fit to the graph, the results shown in Table 3 are obtained. Where N is the number of photons that reached the photo-detector and E is the total energy deposited in the fibers. It can be observed that for this layout the linear relation between the variables is kept (confirmed due to the correlation ≈ 1). However, the parameters of that relation are different that should result from the different fiber arrangement. The fibers' trapping efficiency for this layout, is obtained as before, one plots the graph showing the total number of detected photons as a function of the scintillation photons that were created for the same simulations obtaining the graph in figure 16. From a linear fit to the data the re-

Table 4. Fit results for the total produced photons vs. detected photons relation in the fibers' close-packed layout

$N_d = m \cdot N_p + b$	
m	$0.214714 \pm 9.19411E-05$
b	-53.0323 ± 36.2084
Correlation	≈ 1

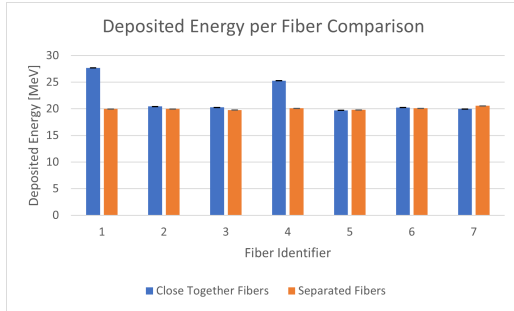


Figure 17. Comparison between the total energy deposited in each fiber in the close-packed layout and the air gap layout with the respective error bar represented in black

Table 5. Comparison between the trapping efficiency of the fibers in their close-packed and air gaps layouts

closed packed Layout	air gaps Layout
$21.488\% \pm 0.009\%$	$21.471\% \pm 0.009\%$

sults in table 4 are obtained. Where N_d is the number of photons that reached the photo-detector and N_p is the number of photons produced in the fibers. Similar to the close-packed layout, the fibers' trapping efficiency is (approximately) independent of the number of protons that hit them, as is equal to the slope of the graph in figure 16 ($21.471\% \pm 0.009\%$)

2.3 Setup comparison

Comparing the total energy deposited in each fiber, one obtains the histogram in figure 17. In this comparison, the most striking difference is in the energy deposited in fibers 1 and 4 for the close-packed layout. While for the air gap layout all fibers have a reasonable agreement. Ignoring those two fibers, the amount of energy deposited in each fiber is approximately the same in both layouts as would be expected. To complete the comparison in table 5 the fibers' trapping efficiency is shown side by side. The difference between the two layouts for the trapping efficiency is 0.017%. A difference that is within the $2 \times 0.009 = 0.018$ error width interval. The conclusion is that the trapping efficiency or the fiber detector efficiency is not changed when one separates the fibres by $25 \mu\text{m}$. Future simulations could be done with a greater separation between the fibers to observe if there is any impact on the trapping efficiency or other quantities related to the signal measured by the individual fibers.

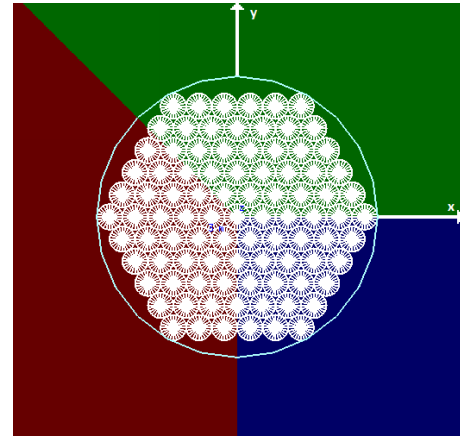


Figure 18. Layout of the fibers in their "big agglomerate" disposition in TOPAS-MC. The Proton beam comes from the right with its center on the x axis. The fibers are numbered to identify them and are circled by a virtual surface whose purpose is only to identify the particles that leave the agglomerate

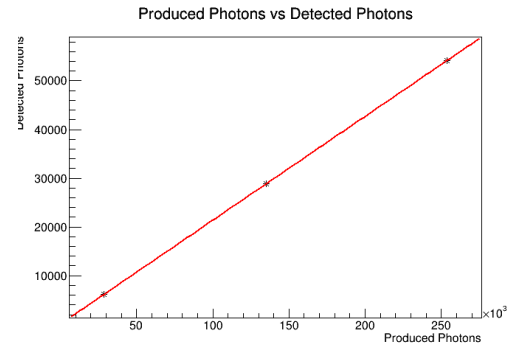


Figure 19. Total photons produced vs. number of photons that reach the detector in the big fibers' closed packed layout.

3 Big agglomerates of fibers

The simulation of fibers agglomerated in a hexagonal structure with a diameter of $275 \mu\text{m}$ followed, as to compare with the fibers commercially available which have the same diameter. For this comparison, a closely packed structure of 91 fibers is used – figure 18. The beam orientation and characteristics are the same.

3.1 Layout's trapping efficiency ratio

Since no change to the scintillation process was included, that analysis is not covered for this layout. The analysis is mainly focused on the trapping efficiency. Plotting the graph of the number of photons detected in function of the number of scintillation photons created for 1k, 5k and 10k protons simulated, the graph in figure 19 is obtained. Performing a linear fit to the graph, the results in table 6 are obtained. Where N_d is the number of photons that reached the photo-detector and N_p is the number of photons produced in the fibers. The trapping efficiency of this layout is slightly smaller than previous layouts by about 0.14%

Table 6. Fit results for the total produced photons vs. detected photons relation in the big fibers' closed packed layout.

$N_d = m \cdot N_p + b$	
m	$0.213307 \pm 5.68691E-05$
b	61.5888 ± 9.48155
Correlation	≈ 1

but still in agreement if the errors are considered being all set within a $2\times$ error interval. The missing data points are due to the higher computation time necessary for these simulations but a very small impact is expected with their inclusion.

4 Conclusions

During the internship, several validation tests were performed. It was possible to validate the implementation of the scintillation process obtaining a linear relation between the deposited energy and the number of scintillation photons created. A trapping efficiency of about 21.48% independent from the number of scintillation photons produced was measured. For the different layouts tested it was shown that this value does not change. The results have also shown unexpectedly a considerable difference in the deposited energy in the different fibers for one of the layouts. A clarification for these differences was not achieved within the internship. The choice of the beam direction along the $-x0x$ might result in messing up the way particles are distributed over the simulated geometry. However the comparison of the close-packed with the air gap layout are confusing. While the first result in a mismatch in the energy distribution the former shows the expected agreement. The results have also shown that the agglomerates with 91 fibers produce considerably fewer scintillation photons than would be expected (as with 10k protons simulated they produced about 250k when the agglomerate with 7 fibers produced 200k in the same conditions). The first preliminary results have shown several issues that need to be understood and solutions implemented. For future simulations with higher statistics and also different

sets of the parameter space (fluence, energy, beam disposition, and characteristics, etc.) should be implemented. A conclusion to the set of preliminary studies are simulations using PMMA separating the SPOFs. The option for this material is because it is considered to be a good substitute for soft tissue and could be used as a supporting structure for micrometric scintillating optical fibers.

Acknowledgements

I would like to thank my supervisors for all the effort they had helping me through this project and for all the support they gave me. I could have never done it without them, as I would just get stressed by all my small mistakes that kept adding up. I would also like to thank my girlfriend for having spent some of her precious time helping me revise the paper and correct some small but important mistakes.

References

- [1] *Provision healthcare*, <https://provisionhealthcare.com/about-proton-therapy/advantages-of-proton/>, accessed: 2022-10-15
- [2] S. Ask, al., NIMA **568**, 588 (2006)
- [3] S. Beddar, L. Beaulieu, *Scintillation Dosimetry, Imaging in Medical Diagnosis and Therapy* (CRC Press, 2016), ISBN 9781482209006, <https://books.google.pt/books?id=UAjYCwAAQBAJ>
- [4] *Total internal reflection*, https://en.wikipedia.org/wiki/Total_internal_reflection, accessed: 2022-10-15
- [5] J. Perl, J. Shin, J. Schümann, B. Faddegon, H. Paganetti, *Med Phys* **39**, 6818 (2012)
- [6] B. Faddegon, J. Ramos-Méndez, J. Schümann, A. McNamara, J. Shin, J. Perl, H. Paganetti, *Phys Med* **72**, 114 (2020)
- [7] *Filmetrics*, <https://www.filmetrics.com/refractive-index-database/Polystyrene/PS>, accessed: 2022-10-15
- [8] *Root*, <https://root.cern/>, version: 6.18.04
- [9] *Paint 3d*, https://apps.microsoft.com/store/detail/paint-3d/9NBLGGH5FV99?hl=pt-br&gl=br&icid=en_US_Store_UH_apps_Win